Dependence of wavefront errors on nonuniformity of thin films

Hongji Qi (齐红基)*, Meiping Zhu (朱美萍), Weili Zhang (张伟丽), Kui Yi (易 葵), Hongbo He (贺洪波), and Jianda Shao (邵建达)

Key Laboratory of Material Science and Technology for High Power Lasers, Shanghai Institute of Optics and Fine Mechanics, Chinese Academy of Sciences, Shanghai 201800, China

**Corresponding author: qhj@siom.ac.cn*

Received April 2, 2011; accepted May 13, 2011; posted online July 29, 2011

In contrast to uncoated substrate, a nonlinear relationship of phase shift with the thicknesses of the thin film makes the calculation of wavefront aberration complicated. A program is compiled to calculate the wavefront aberration of multilayer thin film produced by thickness nonuniformity. The physical thickness and the optical phase change on reflection are considered. As an example, the wavefront aberration of the all-dielectric mirror is presented in ArF excimer lithography system with a typical thickness distribution. In addition, the wavefront errors of the thin film at wavelengths of 193 and 633 nm are compared in the one-piece and two-piece arrangements. Results show that the phase shift upon reflection of the thin film produced by thickness nonuniformity is very sensitive to the incident angle, wavelength, and polarization.

OCIS codes: 310.6870, 000.4430, 050.5080.
doi: 10.3788/COL201210.013104.

In order to prevent the distortion of the beam profile, the perfect flatness specification of surface should be achieved for all the optical components. In a stadium-sized laser facility – National Ignition Facility (NIF) at the Lawrence Livermore National Laboratory – meter-scale laser coatings, e.g., reflector, must meet the wavefront requirement of $\lambda/3$ ($\lambda = 1\ 053$ nm)[1]. Because the phase change is proportional to $1/\lambda$, wavefront control is more difficult for optical components in the ultra-violet (UV) laser system compared with those in the infrared system. In the UV lithographic system, the surface flatness of optical components should be strictly controlled to enhance the exposure resolution in the illumination, imaging, and exposure systems. Compared with the uncoated substrate, the flatness of the coated optical components is determined by more factors[2−6]. In addition, the dependence of wavefront error on nonuniformity must be considered for the meter-scale-size optical components. Ramsay *et al.* investigated the multilayer dielectric reflecting surfaces in Fabry-Perot interferometers[7]. Knowlden calculated the wavefront errors produced by nonuniformity for dielectric-enhanced infrared reflectors[8].

In this letter, on the basis of the "figure error" function module in the Essential Macloed software, a program was compiled to calculate the wavefront aberration due to nonuniformity. The physical thickness and the optical phase change on reflection due to thickness nonuniformity were considered. The calculated results were input into the MetroPro software to construct three-dimentional (3D) surface morphology. As an example, the wavefront aberration of the all-dielectric mirror was presented in ArF lithography system. In addition, the wavefront of the thin film at wavelengths of 193 and 633 nm were compared with nonuniformity of 2%.

For an uncoated optical surface, wavefront distortion is only related to figure error, i.e., the physical thickness modulation of the surface. In the reflection approach, the wavefront error is simply twice that of the surface. In the case of coated optical surface, the phase shift upon reflection of the multilayer thin film is involved in the measurement of wavefront distortion, as shown in Fig. 1. The total phase shift difference, $\Phi_{\rm A}$–$\Phi_{\rm B}$, depends on the physical thickness difference, $d_{\rm A}$–$d_{\rm B}$, and the reflective phase shift difference, $\Phi(d_{\rm A})$–$\Phi(d_{\rm B})$. The phase shift difference $\Delta\Phi$ related to the physical thickness difference, $\Delta d = d_{\rm A}$–$d_{\rm B}$, is given by the formula $\Delta\Phi = \Delta d/\lambda$. The relationship between the reflective phase shift difference $\Phi(d_{\rm A})$–$\Phi(d_{\rm B})$ and the physical thickness difference Δd is relatively complicated.

In the case of isotropic film, the jth layer film can be described by the characteristic matrix $\begin{bmatrix} \cos\delta_j & {\rm i}\sin\delta_j/\eta_j \\ {\rm i}\eta_j\sin\delta_j & \cos\delta_j \end{bmatrix}$, where $\delta_j = \frac{2\pi}{\lambda} n_j d_j \cos\theta_j$ is referred as the phase thickness; n_j and d_j are the refractive index and the physical thickness of the film, respectively; η_j is the effective optical admittance; θ_j is the refractive angle in the jth layer film. Combined with the substrate or emergent medium with effective optical admittance $\eta_{\rm m}$, the characteristic matrix of an assembly of q layers is shown as $\begin{bmatrix} B \\ C \end{bmatrix} = \prod_{j=1}^{q} \begin{bmatrix} \cos\delta_j & {\rm i}\sin\delta_j/\eta_j \\ {\rm i}\eta_j\sin\delta_j & \cos\delta_j \end{bmatrix} \cdot \begin{bmatrix} 1 \\ \eta_m \end{bmatrix}$. Here, B and C are the normalized electric and magnetic fields at the front interface and can be used to extract the properties of the thin film system, including the phase change upon reflection, as shown by the equation

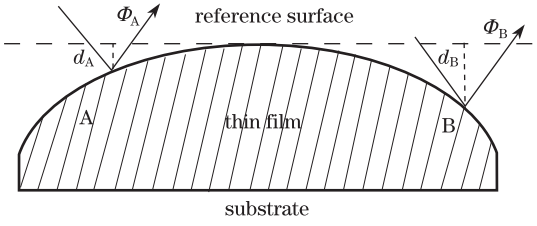

Fig. 1. Physical thickness and phase shift upon reflection produced by nonuniform coating.

$\Phi = \arctan \frac{Im[\eta_m(BC^*-CB^*)]}{(\eta_m^2 BB^*-CC^*)}$ [9]. Due to the nonlinear relationship between the coating thickness and the optical phase change on reflection, the effect of phase shift is dependent on the design and the nonuniformity error of the multilayer thin film.

The all-dielectric reflector used in the discussion is as follows. The fused silica substrate is coated with alternative high-index material (LaF_3) and low-index material (MgF_2). The stack can be shown as G/$(HL)^{15}$ H/A, where G and A denote the fused silica substrate and air, respectively, and H and L are the quarter-wave layers of the index, 1.67 for LaF_3 and 1.41 for MgF_2, respectively. The reference wavelength is 217 nm, while the incident angle is 45°. Figure 2 shows the calculated reflection spectrum (blue curve) and reflectance phase shift (red curve) over 170–700 nm range for s polarization. Similar to the reflection spectrum, the phase shift change over the sideband of the high-reflectance band is abrupt, and the modulation of phase shift decreases for the long-wavelength range far from the high-reflectance band. The phase shift shows a moderate increase over the high-reflectance band.

For the nonuniformity error of –2%, the total wavefront error (orange curve) and that which only considers physical thickness (blue curve) are plotted in Fig. 3. As the above-mentioned analysis, the optical path difference $\Delta\Phi$ related to physical thickness difference Δd is fixed, and the wavefront distortion is

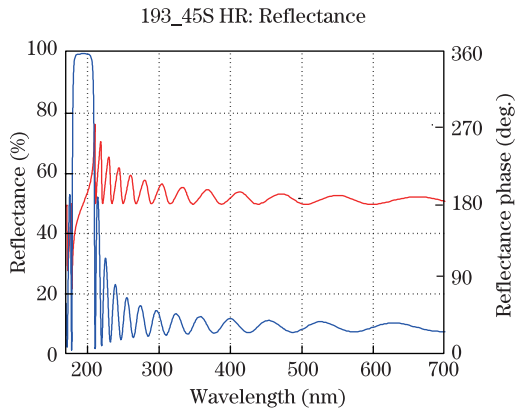

Fig. 2. (Color online) Calculated reflection spectra and phase shift upon reflection for the design G/$(HL)^{15}$ H/A.

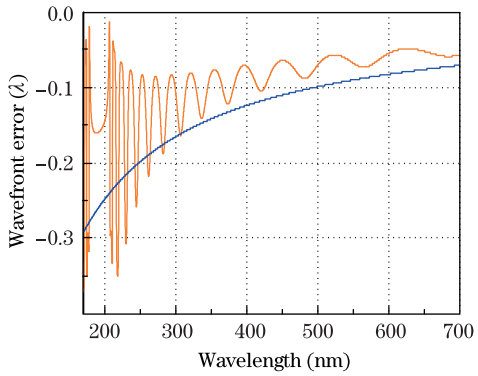

Fig. 3. (Color online) Wavefront error of reflector at the incidence of 45° for s-polarization with nonuniformity error of –2%.

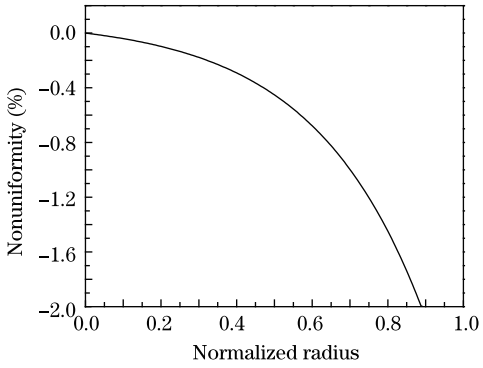

Fig. 4. Uniformity distribution of thin film versus normalized radius for an offset source deposition system.

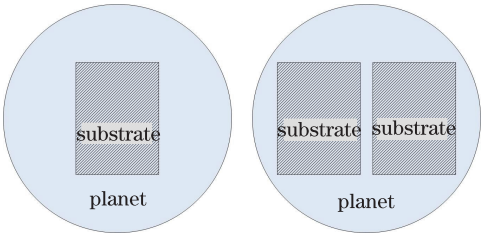

Fig. 5. One-piece and two-piece arrangements of a rectangle optical component with normalized size of 0.7×1.

monotonic function $\Delta\Phi = \Delta d/\lambda$. Because the phase shift is very sensitive to the physical thickness near the sideband of the reflective band, the total phase shift shows abrupt modulation. Over the high-reflectance band, the additional phase shift compensates the phase loss due to the reduction of physical thickness; therefore, the total phase shift at the wavelength of 193 nm is $-0.13\ \lambda$, which is less than $-0.24\ \lambda$, considering only the physical thickness change.

For an offset source deposition system, a radial profile of a typical coating thickness distribution is given in Fig. 4. The normalized radius was used to describe the different sizes of vacuum chamber. The evaporation source of the LaF_3 and MgF_2 materials can be used to deposit the all-dielectric reflector in a vacuum chamber. Here, the same uniformity distribution is assumed for the LaF_3 and MgF_2 materials.

For a rectangle optical component with normalized size of 0.7×1, one or two pieces could be deposited in one planet, as shown in Fig. 5.

In general, one-piece arrangement is preferred in order to restrain the nonuniformity effect of deposited coating. Due to the nonuniformity of the deposited coating, the physical thickness and the phase shift upon reflection of the thin film change with the radial profile. Wavefront data could be calculated with the nonuniformity error of the multilayer thin film. Combined with the head information of the xyz file from Zygo Corporation, a new file including the calculated wavefront data in the xyz format was created. With the commercial MetroPro software, 3D wavefront contour could be constructed. For normal incidence, the constructed wavefront contours are presented in Figs. 6(a) and (b) for wavelengths of 193 and 633 nm, respectively. Because the wavefront is

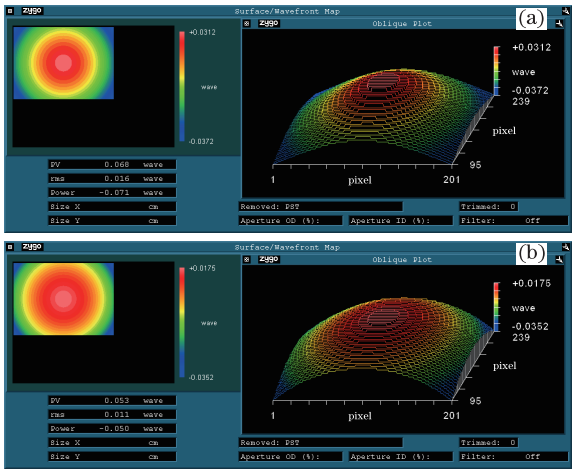

Fig. 6. Constructed wavefront contours of multilayer thin film with the uniformity distribution in Fig. 4 at wavelengths of (a) 193 nm and (b) 633 nm.

Table 1. PV Values of Surface Contour with One-Piece Arrangement

		0°	40° P	45° S
PV at 193 nm	Original (λ)	0.068	0.027	0.037
	Removed Tilt (λ)	0.068	0.027	0.037
	Removed Focus (λ)	0.014	0.002	0.003
PV at 633 nm	Original (λ)	0.053	0.05	0.048
	Removed Tilt (λ)	0.053	0.05	0.048
	Removed Focus (λ)	0.005	0.004	0.004

related to the specified wavelength, and shown in the wavelength unit, the wavefront error should refer to the same wavelength. Therefore, the wavelength parameter was adjusted to 193 nm from 633 nm in Fig. 6(b).

The values of the peak to valley (PV), root mean square (RMS), and power of wavefront contour are 0.068, 0.016, and –0.071 λ in Fig. 6(a), which are different from the 0.053, 0.011, and –0.050 λ in Fig. 6(b). Figure 7 shows the contours for the focal position that yields the minimum RMS wavefront error. The PV values decrease to 0.014 and 0.005 λ, as shown in Figs. 7(a) and (b).

Aside from the wavelength, the incident angle and polarization were also considered in constructing the surface contour. The PV values of the constructed surface contour with the uniformity distribution shown in Fig. 4 at wavelengths of 193 and 633 nm are given in Table 1 for the normal and 45° (two polarizations=45° P and 45° S) oblique incidence. In addition, the PV values of the surface contour with tilt and focus removed are also listed in Table 1.

Due to the rotational symmetry of the thickness distribution on the surface of the optical component for the one-piece arrangement, the PV values before and after removing tilt are the same. Another advantage for such distribution is the perfect PV values of the surface contour after removing focus, decreased by a factor of 5–10 with respect to the original surface contour.

In order to improve the production efficiency, two pieces of optical components with normalized size of 0.7×1 can be deposited in one planet. For the normal incidence, the constructed wavefront contours are presented in Figs. 8(a)–(c) and 8(d)–(f) considering phase shift at wavelengths of 193 and 633 nm, respectively. The PV values of the surface contour before and after removing tilt and focus are listed in Table 2.

Similarly, the surface contours produced by nonuniformity were constructed at normal incidence and 45° incidence for two polarizations. The PV values of the surface contour before and after removing tilt and focus are also listed in Table 2.

As shown in Figs. 8(a) and (c), the rotational symmetry of the surface contour was destroyed and the performance of the surface figure was improved after removing tilt. Compared with the PV values in Table 1, those of the surface contour increased by a factor of 1.7–2.75 and about 2.7 for wavelengths of 193 and 633 nm, respectively. For the data removing tilt and focus, the PV values increased by a factor of 1.6–5.7 and about 5 for wavelengths of 193 and 633 nm, respectively.

Based on the above analysis, the substrate arrangement determines the uniformity distribution of the thin film,

Table 2. PV Values of Surface Contour with Two-Piece Arrangement

		0°	40° P	45° S
PV at 193 nm	Original (λ)	0.115	0.073	0.102
	Removed Tilt (λ)	0.058	0.041	0.057
	Removed Focus (λ)	0.023	0.012	0.017
PV at 633 nm	Original (λ)	0.145	0.132	0.129
	Removed Tilt (λ)	0.082	0.073	0.072
	Removed Focus (λ)	0.025	0.020	0.021

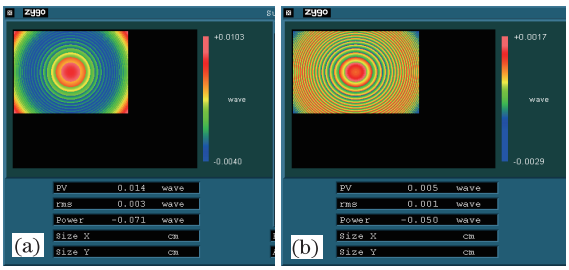

Fig. 7. Zygo interface of surface contour after removing the focus of wavefront contour in Fig. 6.

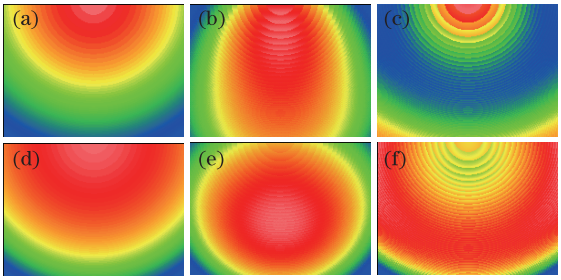

Fig. 8. Simulation results of the surface contour considering phase shift at wavelengths of (a)–(c) 193 nm and (d)–(f) 633 nm. left – original; middle – removing tilt; right – removing tilt and focus.

and the phase shift upon reflection of the thin film produced by nonuniformity is very sensitive to the incident angle, wavelength, and polarization. The surface figure of the optical component should be measured at the used incident angle, wavelength, and polarization.

In conclusion, for multilayer thin film, the phase shift upon reflection has a nonlinear relationship with physical thickness. The physical thickness and the optical phase change on reflection due to thickness nonuniformity are considered to caculate the wavefront aberration with the compiled program. The results show that the phase shift upon reflection of the thin film produced by nonuniformity is very sensitive to the incident angle, wavelength, and polarization. Therefore, the surface wavefront of the optical component should be measured at the used incident angle, wavelength, and polarization.

This work was supported by the National Natural Science Foundation of China under Grant Nos. 60878045 and 10976030.

References

1. W. Williams, "NIF large optics metrology software: description and algorithms," (Lawrence Livermore National Laboratory (LLNL), Livermore, CA, 2002).
2. J. R. Piascik, J. Y. Thompson, C. A. Bower, and B. R. Stoner, J. Vacuum Sci. & Technol. A **23,** 1419 (2005).
3. M. Niibe, H. Nii, and Y. Sugie, Jpn. J. Appl. Phys. **41,** 3069 (2002).
4. D. W. Reicher and S. A. McCormack, Proc. SPIE **4091,** 104 (2000).
5. Q. Xiao, H. He, S. Shao, J. Shao, and Z. Fan, Thin Solid Films **517,** 4295 (2009).
6. Y. Wang, Y. Zhang, W. Chen, W. Shen, X. Liu, and P. Gu, Appl. Opt. **47,** C319 (2008).
7. J. Ramsay and P. Ciddor, Appl. Opt. **6,** 2003 (1967).
8. R. Knowlden, Proc. SPIE **288,** 78 (1981).
9. H. A. Macleod, *Thin-Film Optical Filters* (3rd ed.), (Institute of Physics Pub., Philadelphia, 2001).